Heterogeneous reaction of NO$_2$ with hematite, goethite and magnetite: Implications for nitrate formation and iron solubility enhancement

Rui Li [a, d], Xiaohong Jia [a, d], Fu Wang [b], Yan Ren [b], Xiao Wang [a, d], Huanhuan Zhang [a, d], Guanghui Li [c], Xinming Wang [a, d, e], Mingjin Tang [a, d, e, *]

[a] State Key Laboratory of Organic Geochemistry and Guangdong Key Laboratory of Environmental Protection and Resources Utilization, Guangzhou Institute of Geochemistry, Chinese Academy of Sciences, Guangzhou 510640, China
[b] Longhua Center for Disease Control and Prevention of Shenzhen, Shenzhen 518109, China
[c] Institute for Environmental and Climate Research, Jinan University, Guangzhou 511443, China
[d] University of Chinese Academy of Sciences, Beijing 100049, China
[e] Center for Excellence in Regional Atmospheric Environment, Institute of Urban Environment, Chinese Academy of Sciences, Xiamen 361021, China

HIGHLIGHTS

- Exposure to NO$_2$ led to surface deactivation of hematite, magnetite and goethite.
- More nitrate was formed on goethite when compared to hematite and magnetite.
- Impacts of this reaction on nitrate aerosol formation and iron solubility may be very limited.

ARTICLE INFO

ABSTRACT

Atmospheric processing may significantly increase solubility of iron in mineral dust, but the effects of heterogeneous reactions on iron solubility have been poorly understood. In this work, we investigated heterogeneous reaction of NO$_2$ (15 ± 1 and 2.5 ± 0.1 ppmv, equal to ~3.7 × 10^{14} and ~6.2 × 10^{13} molecule cm^{-3}) with hematite, magnetite and goethite at different relative humidities (RH, 0–90%), and changes in particulate nitrate and soluble iron due to heterogeneous reaction with NO$_2$ were quantified as a function of time (up to 24 h). After reaction with 2.5 ± 0.1 ppmv NO$_2$ for 24 h (or less time), hematite and magnetite were fully saturated, while goethite was only partly deactivated. Nitrate yield was largest for goethite, and the mass ratio of formed nitrate to unreacted mineral only reached ~1% or less after 24 h reaction. All the three minerals showed low reactivities towards NO$_2$, and the average reactive uptake coefficients of NO$_2$ in the first 3 h were found to be < 5 × 10^{-8}. In addition, the increase in iron solubility was found to be small and in some cases even insignificant for the three minerals after heterogeneous reaction with NO$_2$ for 24 h. Overall, the impacts of heterogeneous reaction of NO$_2$ with hematite, magnetite and goethite on nitrate aerosol formation and iron solubility could be very limited.

© 2019 Elsevier Ltd. All rights reserved.

1. Introduction

Every year approximately 2000 Tg mineral dust is emitted into atmosphere, contributing to a large fraction of tropospheric aerosol particles globally (Huneeus et al., 2011; Ginoux et al., 2012). Mineral

dust aerosol has significant impacts on tropospheric chemistry (Dentener et al., 1996; Usher et al., 2003; Tang et al., 2017) and climate (Cziczo et al., 2013; Tang et al., 2016; Kok et al., 2018). Furthermore, deposition of mineral dust is a major source of iron for surface waters in many open ocean regions where iron is a limiting micronutrient for phytoplankton growth (Jickells et al., 2005; Mahowald et al., 2005; Schulz et al., 2012; Hettiarachchi et al., 2018a), and hence largely controls primary productivity and biogeochemical cycles in these regions (Boyd et al., 2007, 2010; Mahowald, 2011; Tagliabue et al., 2017). In addition to mineral dust,

combustion aerosol may also be an important source of iron in oceanic regions (Luo et al., 2008; Ito et al., 2019).

In mineral dust aerosol, Fe-bearing minerals include crystalline iron oxides (Lafon et al., 2004; Shi et al., 2009), such as goethite, hematite and magnetite, ferrihydrite and poorly crystalline Fe (Shi et al., 2009), and clay minerals (Avila et al., 1997; Shi et al., 2005; Journet et al., 2008), such as kaolinite, illite and montmorillonite. Most of the iron contained in the mineral dust is highly refractory, and only a small fraction is soluble/bioavailable (Shi et al., 2012; Sholkovitz et al., 2012; Mahowald et al., 2018). Many studies (Baker et al., 2006; Shi et al., 2011a; Sholkovitz et al., 2012; Mahowald et al., 2018) have found that the apparent iron solubility in aerosol particles collected in remote marine areas is higher than those collected near desert source regions. Several processes could be responsible for the observed increase in iron solubility with atmospheric transport (Journet et al., 2008; Solmon et al., 2009; Ooki et al., 2009; Schroth et al., 2009; Cartledge et al., 2015), including chemical aging in the troposphere. For example, previous work (Shi et al., 2009, 2012; Fu et al., 2012; Chen and Grassian, 2013; Wang et al., 2017, 2018) found that aqueous reactions (i.e. cloud processing) would significantly increase iron solubility of mineral dust.

Heterogeneous reactions would affect the abundance of a number of trace gases both directly and indirectly (Dentener et al., 1996; Bedjanian et al., 2013; Tang et al., 2017). These reactions can also modify chemical composition (Laskin et al., 2005; Sullivan et al., 2007; Ma et al., 2012) and thus physicochemical properties of mineral dust (Krueger et al., 2003; Kulkarni et al., 2015; Tang et al., 2016). Heterogeneous reaction of NO_2 with mineral dust is of particulate interest, as it may contribute directly to the NO_2 removal and the formation of nitrate aerosol and HONO (Underwood et al., 1999; Ndour et al., 2008; Li et al., 2010; Liu et al., 2015; Kebede et al., 2016; Tan et al., 2016), and would then indirectly impact the abundance of OH radicals and volatile organic compounds as HONO photolysis is an important source of OH radicals. For example, Underwood et al. (1999) used transmission FTIR and a Knudsen-cell reactor to investigate heterogeneous reactions of NO_2 with Al_2O_3, Fe_2O_3 and TiO_2, and nitrate (as well as nitrite) was found on particles; in addition, the initial uptake coefficients were reported to be $< 1 \times 10^{-6}$. Significant amount of particulate nitrate was found in heterogeneous reaction of NO_2 with $CaCO_3$ (Li et al., 2010), and the uptake coefficients increased with RH. A coated-wall flow tube was employed by Liu et al. (2015) to study heterogeneous reactions of NO_2 with Fe_2O_3 and kaolinite, and found that increase in relative humidity (RH) would led to decrease in initial uptake coefficients and increase in HONO yields.

Furthermore, heterogeneous uptake of NO_2 onto mineral dust can be photo-enhanced (Ndour et al., 2008; Kebede et al., 2016). However, the effects of heterogeneous reactions on iron solubility of mineral dust have been rarely explored, though a number of previous studies investigated how aqueous reactions would modify iron solubility of mineral dust (Shi et al., 2012, and references therein). Baltrusaitis et al. (2012) showed that heterogeneous reaction with NO_2 would largely increase water solubility of Pb in PbO particles, and one may expect this reaction would also lead to significant enhancement in iron solubility in mineral dust particles. However, this hypothesis is yet to be verified and quantified. We note that a recent study (Cartledge et al., 2015) found that heterogeneous reactions with SO_2 did not significantly increase iron solubility for hematite, magnetite and goethite. To our knowledge, this is the first study which explored the impact of heterogeneous reactions on the solubility of iron contained in mineral dust.

In the present work, we investigated heterogeneous reaction of NO_2 with hematite, magnetite and goethite at different relative humidities (RH, 0–90%), and measured the change in particulate nitrate and soluble iron as a function of reaction time (up to 24 h)

under atmospherically relevant conditions. The first motivation of our work is to elucidate whether and to which extent heterogeneous reaction with NO_2 would increase iron solubility of mineral dust. The second motivation is to assess the contribution of this reaction to nitrate aerosol formation, as the uptake coefficients reported by previous studies display large discrepancies (Crowley et al., 2010), and such discrepancies can result from experimental conditions used (e.g., particles used investigation were prepared).

2. Experimental sections

2.1. Sample preparation and characterization

In this work heterogeneous reaction of hematite (>99.8%, Strem Chemicals, Inc., USA), magnetite (>95%, Strem Chemicals, Inc., USA) and goethite (>98%, Santa Cruz Biotechnology, USA) with NO_2 was investigated. The BET (Brunauer-Emmett-Teller) volumetric surface areas of these minerals were measured by nitrogen absorption at 77 K, using an ASAP 2640 Accelerated Surface Area and Porosimetry Analyzer (Micromeritics, USA). Prior to analysis, ~800 mg particles were degassed at 413 K under a He gas flow for at least 3 h. The BET surface areas were determined to be 9.23 ± 0.17, 6.34 ± 0.04 and $11.30 \pm 0.08 \, m^2 \, g^{-1}$ for hematite, magnetite and goethite.

For each iron containing mineral, ~0.25 g minerals were mixed with 500 mL HPLC-grade ethanol (Kermel Chemical Regent, China) and stirred using a magnetic stirrer, and the mass concentration of minerals in the aqueous mixture was ~0.5 g/L. A pipette was used to transfer 10 mL aqueous mixture onto a PTFE filter (47 mm, Whatman, USA), and mineral-loaded filters were weighted after complete evaporation of ethanol. Visual inspection revealed that mineral particles were uniformly distributed on filters, and the mass of particles on each filter was 5 ± 1 mg, suggesting good reproducibility of samples prepared.

The morphology of iron minerals loaded on filters was characterized using a SU8010 cold field emission scanning electron microscope (Hitachi, Tokyo, Japan) operated at an accelerating voltage of 1–1.5 kV, and an X-ray energy-dispersive spectrometer (EDS) was coupled with the scanning electron microscope (SEM) to measure elemental compositions. A small piece of particle-loaded filter (about 0.8 cm × 0.5 cm) was mounted on the SEM stub by a double-sided carbon tape and coated with a thin gold layer. Due to its ferromagnetism, it was technically more difficult to analyze magnetite using SEM, and thus only the morphology and elemental composition of hematite and goethite were characterized. SEM measurements revealed that most particles were in the diameter range of 0.2–0.5 μm for hematite and goethite (Figs. S1-S2); in addition, we employed dynamic light scattering to characterize the three minerals, and the average particle diameters were measured to be 0.8, 1.0 and 1.7 μm for hematite, goethite and magnetite (Fig. S3). Because hematite and goethite particles were irregular, particle diameters measured using two different techniques were consistent. If we assume that particles are spherical with a uniform diameter of 0.4 μm and a density of 5 g cm^{-3} (equal to the density of hematite), it was estimated that 2–3 layers of particles were deposited on the filter.

2.2. Heterogeneous reactions

Fig. 1 displays the schematic diagram of the apparatus used to investigate heterogeneous reactions of NO_2 with mineral dust particles. A small flow of NO_2 (1000 ppmv in air, National Institute of Metrology, Beijing, China) was mixed with a dry synthetic air (>99.999%, Huate Gas Co., Ltd, Foshan, China) flow and a humidified synthetic air flow, which was humidified by passing a dry synthetic air flow through two water bubblers in series. All the three flows
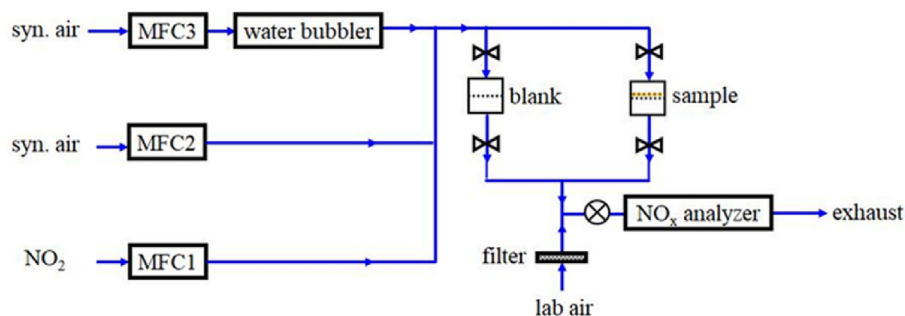
Fig. 1. Schematic diagram of the apparatus used to investigate heterogeneous reaction of NO_2 with mineral dust particles. MFC1, MFC2 and MFC3 were mass flow controllers. The two synthetic air flows, controlled using MFC2 and MFC3, had a total flow rate of 350 sccm; the NO_2 flow, controlled using MFC1, had a flow rate in the range of 0−10 sccm; the NOx analyzer had a flow rate of 500 ± 50 ccm.

were regulated using mass flow controllers (Sevenstar electronics Co., Beijing, China). The dry and humidified synthetic air flows (regulated using MFC2 and MFC3) had a total flow rate of 350 sccm (standard cubic centimeter per min).

The gas mixture was first passed through the left chamber in which a blank filter was housed. When the NO_2 concentration became stable, the gas mixture was then passed through the right chamber in which a mineral-loaded filter was housed so that the reaction was initiated. In order to terminate the reaction, the gas mixture was passed through the left chamber again, and then the particle-loaded filter was taken out for further analysis. The filter was then immediately stored in a sealed plastic box to avoid contamination and reaction with lab air, and was usually dissolved in proper solutions (see Section 2.3 for more details) within 30 min. In this work, the maximum reaction time was 24 h. The two reaction chambers were identical, having an inner diameter of 41.5 mm, an inner length of 87 mm and thus an inner volume of 118 mL. The average residence time was calculated to be ~18 s under a flow rate of 350 sccm. The chamber was divided to two identical parts by the filter, and the gas flow was transferred through the filter to ensure that all the particles loaded on the filter were exposed to NO_2. Chambers were made of aluminum, and the inner surface was coated with fluorinated ethylene propylene (FEP) to minimize wall loss.

As shown in Fig. 1, after exiting the chamber, the gas mixture was further diluted by lab air (filtered using a 47 mm PTFE filter supplied by Whatman) to a total flow of 500 ± 50 ccm (cubic centimeter per min) and then sampled into a NOx analyzer (Model T200, Teledyne Instruments, USA) to monitor NO_2 concentrations online. We used two different NO_2 concentrations (15 ± 1 and 2.5 ± 0.1 ppmv) to explore the effect of NO_2 concentration on heterogeneous reaction, and NO_2 concentrations in the reaction chamber were calculated from the measured NO_2 concentrations after taking into account dilution by filtered lab air, and the dilution factor was 1.22. The NO_2 concentration in the filtered lab air was typically <0.1 ppmv, and therefore its influence on the measured NO_2 concentration (a few ppmv) was negligible. In our work, the relative deviation of NO_2 concentrations from set values was smaller than 10%.

2.3. Analysis

After the reaction, the filter was divided to two halves using acid-washed ceramic-bladed scissors. One half of the filter was extracted in 10 mL deionized water for 2 h using an orbital shaker; after that, the extract was filtered using a 0.22 μm polyethersulfone filter (Anpel, Shanghai, China) and then analyzed using ion chromatography (761 Compact IC, Metrohm, Switzerland) equipped

with a Metrohm suppressor Module and a Metrohm Metrosep A sup 5-250 column. The eluent (4.8 mM Na_2CO_3 and 1.5 mM $NaHCO_3$) and the regenerant (50 mM H_2SO_4) both had a flow rate of 0.7 mL min^{-1}. For each measurement, 100 μL solution was injected through the injection loop.

The other half of the filter was extracted in 10 mL sodium acetate buffer solution (5 mM, pH = 4.18) for 2 h using an orbital shaker, and the extract was also filtered using a 0.22 μm polyethersulfone filter. Many previous studies (Baker et al., 2006; Baker and Croot, 2010; Shi et al., 2011a, 2013; Sholkovitz et al., 2012; Morton et al., 2013; Cartledge et al., 2015) used similar operational methods to extract soluble iron, as these leaching solutions (such as acetate buffer used in our work) could simulate marine precipitation. After that, the filtrate was acidified with 59 μL HNO_3 (>69% v/v, Chron Chemicals, China), and nitric acid concentration in the resulting solution was ~0.4% v/v. An inductively coupled plasma-mass spectrometer (ICP-MS, iCAP Q, Thermo Fisher Scientific, USA) was used to determine the total iron concentration (the sum of Fe^{2+} and Fe^{3+}) in the solution. Measurements were carried out in the single collision cell mode with kinetic energy discrimination, and pure He was used as collision gas. To ensure measurement reliability, yttrium was used as an inner standard; in addition, each solution sample was measured for three times, and the average value was reported.

3. Results and discussion

3.1. Change in surface elemental composition

The morphology and surface elemental composition of hematite and goethite before and after heterogeneous reaction with NO_2 are shown in Fig. 2 and Figs. S1-S2 in the supplement, and there was no obvious difference in particle morphology before and after the reaction. As shown in Fig. 2a−b, both hematite and goethite particles were rather homogeneously deposited on filters. Fig. 2c−d shows EDS spectra of hematite particles before and after the reaction. Compared to unreacted hematite particles, a small but significant nitrogen peak appeared in the EDS spectrum of reacted particles, suggesting that nitrogen-containing species (to be more specific, nitrate) were formed due to heterogeneous reaction with NO_2. In addition, as revealed by EDS observation (not shown), nitrate was also formed on goethite particles after heterogeneous reaction with NO_2.

3.2. Nitrate formation

While mechanisms are very complicated at the molecular level for heterogeneous reaction of mineral dust with NO_2, the major
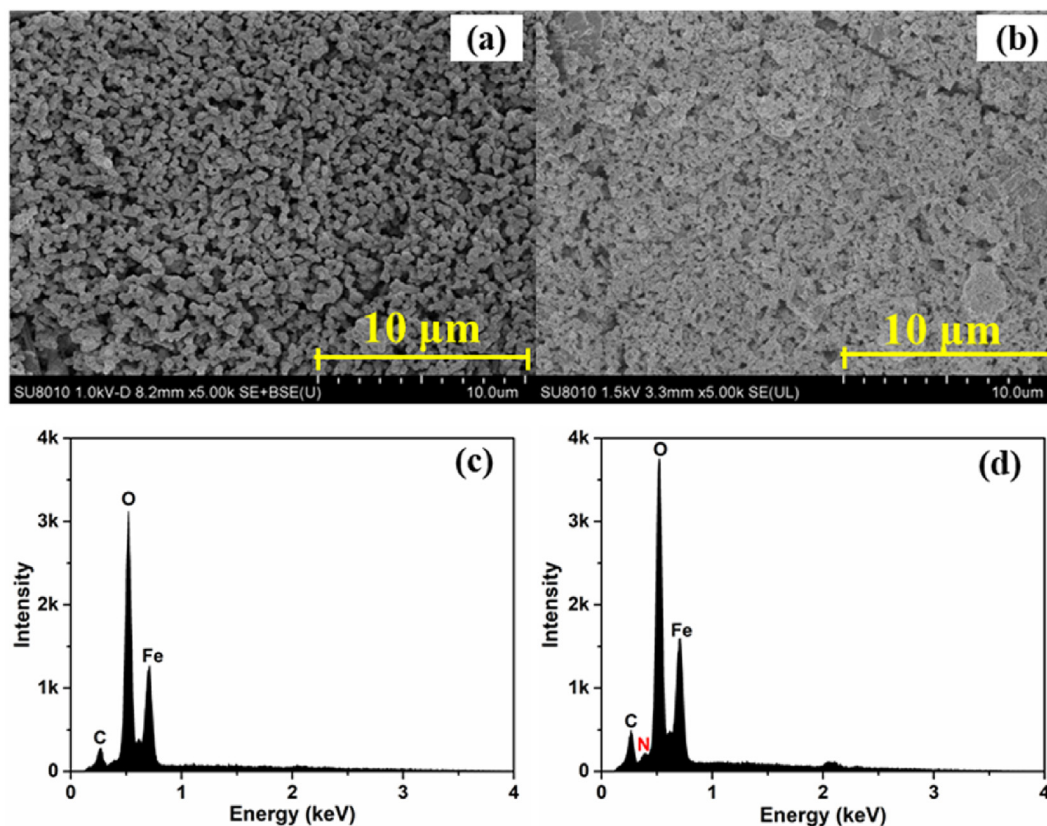
Fig. 2. (a) SEM image of unreacted hematite; (b) SEM image of unreacted goethite; (c) EDS spectrum of hematite before heterogeneous reaction with NO_2; (d) EDS spectrum of hematite after heterogeneous reaction with 2.5 ppmv NO_2 for 24 h at 90% RH.

mechanism can be overall described by (R1) (Underwood et al., 1999; Baltrusaitis et al., 2009; Li et al., 2010; Liu et al., 2015; Liu et al., 2017):

$$NO_2(g) + NO_2(g) \rightarrow HNO_3(ad) + HONO\ (g)\ (R1)$$

In the particles, the predominant product was found to be nitrate (NO_3^-) and nitrite (NO_2^-) was usually minor (Underwood et al., 1999; Baltrusaitis et al., 2009; Li et al., 2010), and HONO was identified as a major product in the gas phase (Liu et al., 2015). In our work ion chromatography was used to measure compositional change of hematite, magnetite and goethite after heterogeneous reaction with NO_2. Similar to previous work, nitrate (NO_3^-) formation was observed for the three minerals, while particulate nitrite (NO_2^-) was not detected, probably because nitrite formed mainly partitioned in the gas phase as HONO. However, we did not attempt to measure HONO in our work.

3.2.1. Hematite

Fig. 3 shows particulate nitrate formation for heterogeneous reaction of hematite with 15 ± 1 ppmv NO_2 at 0%, 30%, 60% and 90% RH as a function of reaction time. At 0%, 30% and 60% RH, the mass fraction of formed nitrate, $m(NO_3^-)/m$, defined as the ratio of the mass of formed nitrate to the initial mass of mineral particles, reached the plateau after 3 h reaction and did not further increase with time. This suggested that hematite surface was saturated in 3 h (or even less) after exposure to 15 ± 1 ppmv NO_2 at 0%, 30% and 60% RH. In addition, very similar amounts of nitrate were formed at 0%, 30% and 60% RH, with average $m(NO_3^-)/m$ being 0.18 ± 0.03%.

Compared to that at 0−60% RH, heterogeneous reaction with NO_2 showed a slightly different picture at 90% RH. As displayed in
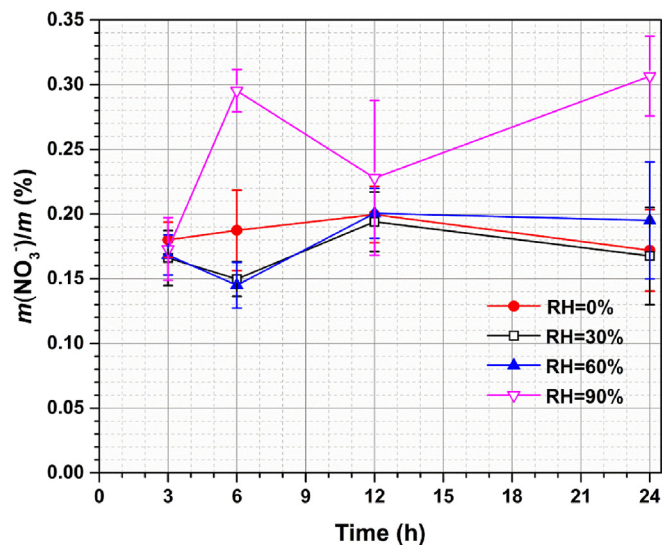

Fig. 3. Nitrate formation in heterogeneous reaction of hematite with 15 ± 1 ppmv NO_2 at 0%, 30%, 60% and 90% RH.

Fig. 3, $m(NO_3^-)/m$ increased from 0.17 ± 0.02% after 3 h to 0.30 ± 0.02% at 6 h, though further increase in reaction time to 24 h did not lead to additional nitrate formation. Compared to reactions at lower RHs (0%, 30% and 60%), significantly more nitrate was formed on hematite due to heterogeneous reaction with NO_2: the maximum $m(NO_3^-)/m$ values were 0.31 ± 0.03% at 90% RH and 0.20 ± 0.02% at lower RH. This suggested that increase in RH from

60% to 90% would enhance heterogeneous reaction of hematite with NO_2.

As hematite was deactivated rather quickly when the NO_2 concentration was 15 ± 1 ppmv, we further examined heterogeneous reaction with NO_2 at a lower NO_2 concentration (2.5 ± 0.1 ppmv), and the results are displayed in Fig. 4. For the reaction under three lower RHs (0%, 30% and 60%), the following differences were observed at high and low NO_2 concentrations. First, particulate nitrate continued to grow until reaction for 12 h, i.e. hematite surface was deactivated after 12 h reaction. Second, the maximum value of $m(NO_3^-)/m$ was $0.16 \pm 0.02\%$ when NO_2 concentration was 2.5 ± 0.1 ppmv, smaller than that $0.20 \pm 0.02\%$ when NO_2 concentration was 15 ± 1 ppmv. For lower NO_2 concentration (2.5 ± 0.1 ppmv), at 90% RH the amount of formed nitrate reached $0.20 \pm 0.06\%$ after reaction for 24 h and was still increasing, further confirming that increase in RH from 60% to 90% would promote heterogeneous reaction of NO_2 with hematite. Previous work (Goodman et al., 2001; Ma et al., 2010; Tang et al., 2016) suggested that increase in RH would lead to more surface-adsorbed water, and thus more nitrate was formed at 90% RH, when compared to that at 60% RH. Nevertheless, Fig. 4 revealed that the formation rate of nitrate at 90% RH decreased with time. As experiments conducted at lower NO_2 concentration are more atmospherically relevant, we only examined heterogeneous reaction of magnetite and goethite at low NO_2 concentration (2.5 ± 0.1 ppmv).

Two previous studies investigated heterogeneous reaction of NO_2 with Fe_2O_3 (Underwood et al., 1999; Liu et al., 2015). A Knudsen cell reactor was used to explore heterogeneous uptake of NO_2 ($0.01-10$ ppmv) onto Fe_2O_3 under dry conditions (Underwood et al., 1999), and a coated wall flow tube was used to examine heterogeneous reaction of NO_2 (0.15 ppmv) with hematite at $7-74\%$ RH (Liu et al., 2015). Similar to our work, complete deactivation of Fe_2O_3 surface was also observed in the two previous studies.

3.2.2. Magnetite

Fig. 5 shows particulate nitrate formation in heterogeneous reaction of magnetite with 2.5 ± 0.1 ppmv NO_2 at 30% and 60% RH as a function of reaction time. At both RHs, the mass fraction of formed nitrate did not further increase with time after reaction for 3 h, suggesting that magnetite surface was deactivated in 3 h or less. In addition, similar amounts of nitrate were formed at two RHs, and
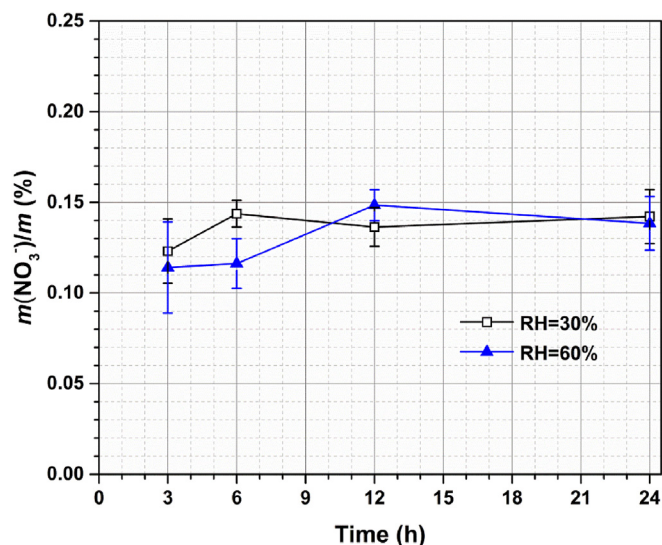
Fig. 5. Nitrate formation in heterogeneous reaction of magnetite with 2.5 ± 0.1 ppmv NO_2 at 30% and 60% RH.

the average $m(NO_3^-)/m$ was determined to be $0.13 \pm 0.02\%$. For comparison, under the same condition $m(NO_3^-)/m$ was found to be $0.10 \pm 0.04\%$ for hematite, slightly lower than that for magnetite.

Two additional experiments were conducted to measure the amount of nitrate formed after heterogeneous reaction of magnetite with 2.5 ± 0.1 ppmv NO_2 for 24 h at 90% RH, and the average $m(NO_3^-)/m$ was determined to $0.20 \pm 0.06\%$, larger than that at 30% and 60% RH. As a result, increase in RH from 60% to 90% could also promote heterogeneous reaction of NO_2 with magnetite.

3.2.3. Goethite

Particulate nitrate formation is displayed in Fig. 6 as a function of time for heterogeneous reaction of goethite with 2.5 ± 0.1 ppmv NO_2 at 30% and 60% RH. Under these conditions, goethite surface was not fully saturated after 24 h reaction, though the formation rate of nitrate decreased with time. The mass fraction of formed nitrate reached $0.83 \pm 0.13\%$ at 30% RH and $1.00 \pm 0.11\%$ at 60% RH
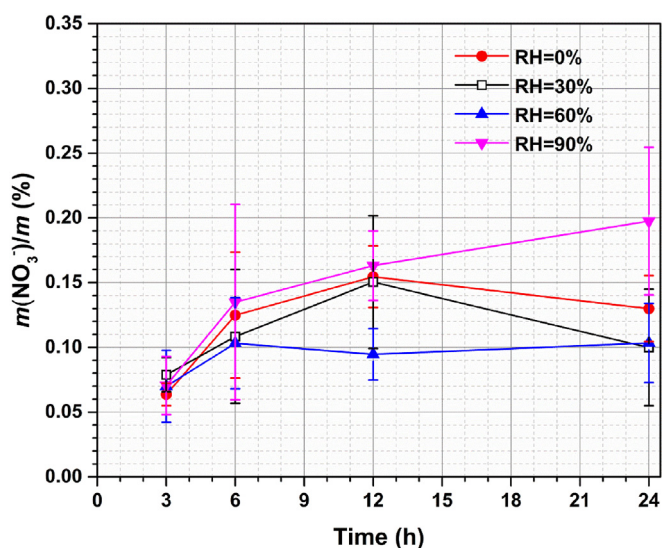
Fig. 4. Nitrate formation in heterogeneous reaction of hematite with 2.5 ± 0.1 ppmv NO_2 at 0%, 30%, 60%, and 90% RH.
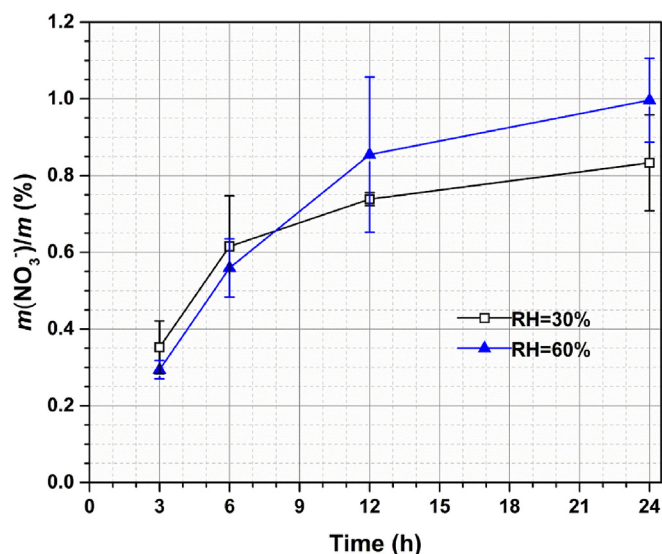
Fig. 6. Nitrate formation in heterogeneous reaction of goethite with 2.5 ± 0.1 ppmv NO_2 at 30% and 60% RH.

for goethite, much larger than those for hematite and magnetite under the same conditions (by a factor of >5). This suggested that compared to hematite and magnetite, goethite was more reactive toward NO_2. In addition, increasing RH from 30% to 60% led to more nitrate formed for goethite, while enhancement in nitrate formation was only observed for hematite and magnetite when RH was increased from 60% to 90%.

3.2.4. Uptake kinetics and surface coverage of formed nitrate

The reactive uptake coefficient, $\gamma(NO_2)$, is defined as the number of reactive collisions leading to the formation of nitrate per second, $d[NO_3^-]/dt$, divided by the frequency of total collisions (Z) between NO_2 and the mineral surface (Li et al., 2006; Tan et al., 2016):

$$\gamma(NO_2) = \frac{d[NO_3^-]}{dt} \bigg/ Z \tag{1}$$

$$Z = 0.25 . A_s . [NO_2] . c(NO_2) \tag{2}$$

where A_s is the surface area of particles (equal to the BET surface area of mineral particles multiplied by their mass used in an experiment), $[NO_2]$ is the number concentration of NO_2, $c(NO_2)$ is the mean molecular speed of NO_2 ($37043\,cm\,s^{-1}$, 298 K). As the shortest reaction time was 3 h in our study, we reported the average $\gamma(NO_2)$ in the first 3 h, and the results are compiled in Table 1.

As shown in Table 1, overall heterogeneous reactivity of hematite, magnetite and goethite towards NO_2 was rather low, and the average $\gamma(NO_2)$ in the first 3 h were found to be $< 5 \times 10^{-8}$. When the NO_2 concentration was 2.5 ± 0.1 ppmv, at the same RH $\gamma(NO_2)$ were largest for goethite and smallest for hematite. In addition, heterogeneous reaction of NO_2 with hematite was conducted at two different NO_2 concentrations, and as shown in Table 1, increase in NO_2 concentration led to decrease in $\gamma(NO_2)$. To our knowledge, heterogeneous reaction of NO_2 with magnetite and goethite has not been explored before.

Underwood et al. (1999) used a Knudsen cell to investigate heterogeneous uptake of NO_2 onto Fe_2O_3 under dry conditions, and the initial $\gamma(NO_2)$, after taking into account bulk diffusion, was determined to be 7×10^{-7}. The steady-state $\gamma(NO_2)$ onto hematite, determined using a coated wall flow tube, were found to be $(1.2-1.5) \times 10^{-8}$ for RH in the range of 7−74% (Liu et al., 2015). For comparison, when NO_2 concentration was 2.5 ± 0.1 ppmv, the average $\gamma(NO_2)$ in the first 3 h was found to be $\sim 1.2 \times 10^{-8}$ for hematite at 0−90% RH in our work. Therefore, the average $\gamma(NO_2)$ determined in our work are in good agreement with those reported by Liu et al. (2015), while much smaller (by a factor of >50) than the initial $\gamma(NO_2)$ measured by Underwood et al. (1999). As Fe_2O_3 surface was gradually deactivated during heterogeneous uptake of NO_2, the initial $\gamma(NO_2)$ is expected to be larger than the average and steady-state $\gamma(NO_2)$. In addition, our work found that the average $\gamma(NO_2)$ exhibited no dependence on RH, and Liu et al. (2015) also suggested the effect of RH on the steady-state $\gamma(NO_2)$ was insignificant.

As the three minerals considered in our work had different BET surface areas, we further compared surface coverages of formed nitrate, i.e. by normalizing formed nitrate to the particle surface area. The surface coverage (θ) of nitrate formed on mineral surface can be calculated using Eq. (3) (Tang et al., 2016):

$$\theta = \frac{m(NO_3^-)}{m(mineral)} . \frac{N_A . A(NO_3^-)}{M(NO_3^-) A_{BET}} \tag{3}$$

where $m(NO_3^-)$ and $m(mineral)$ are the mass (g) of nitrate and mineral, N_A is the Avogadro constant ($6.02 \times 10^{23}\,mol^{-1}$), $M(NO_3^-)$ is the molar mass of nitrate ($62\,g\,mol^{-1}$), A_{BET} is the BET surface area of mineral, and $A(NO_3^-)$ is the average surface area of one nitrate ion, assumed in this study to be equivalent to that for surface-adsorbed water ($1 \times 10^{-15}\,cm^2$) (Tang et al., 2016). The maximum surface coverages of formed nitrate were calculated to be 0.32 ± 0.03, 0.22 ± 0.01 and 0.84 ± 0.09 for hematite, magnetite and goethite, indicating that not all the surface sites were reactive towards NO_2. The maximum surface densities of nitrate were determined to be $(3.22 \pm 0.32) \times 10^{14}$, $(2.16 \pm 0.13) \times 10^{14}$ and $(8.39 \pm 0.92) \times 10^{14}\,cm^{-2}$ for hematite, magnetite and goethite. In a previous study (Underwood et al., 1999), the surface density of nitrate was determined to be $(1.5-2) \times 10^{14}\,cm^{-2}$ for hematite at the steady state under dry conditions, agreeing reasonably well with that measured in our work. Among the three Fe-containing minerals examined, goethite showed highest reactivity towards NO_2, mainly because goethite contains substantial amount of OH groups (Wijenayaka et al., 2012) which are very reactive towards NO_2 (Liu et al., 2017).

3.3. Impacts on iron solubility

The concentrations of soluble iron in extracts of unreacted hematite, magnetite and goethite were measured to be 0.78 ± 0.83, 12.40 ± 0.82 and $21.76 \pm 2.95\,\mu g\,L^{-1}$. Please note that soluble iron concentration in the extract of unreacted hematite was below the detection limit ($1.00\,\mu g\,L^{-1}$). Consequently, iron fractional solubility, defined as the ratio of soluble Fe to the total Fe, was determined to be $(0.4 \pm 0.5) \times 10^{-5}$, $(7.2 \pm 0.4) \times 10^{-5}$ and $(13.6 \pm 1.6) \times 10^{-5}$ for hematite, magnetite and goethite. Shi et al. (2011b) used ammonium acetate buffer (pH = 4.7) to dissolve soluble iron in Sahara dust, and the iron fractional solubility was found to be in the range of $(1-8) \times 10^{-3}$ (0.1−0.8%). Although very similar extraction methods were adopted by Shi et al. (2011b) and our work, fractional solubilities reported by Shi et al. (2011b) were almost two orders of magnitude larger than those measured in our work. This is mainly because Saharan dust contains minerals (such as clay minerals) with much larger iron fractional solubilities (Journet et al., 2008; Hettiarachchi et al., 2018b, Hettiarachchi et al., 2019), when compared to iron oxides and oxyhydroxides.

Fig. 7 displays changes in iron fractional solubility due to heterogeneous reaction with NO_2 as a function of reaction time at different RH. As shown in Fig. 7a−b, heterogeneous reaction with NO_2 would slightly increase the iron fractional solubility for hematite. Furthermore, reaction with 15 ± 1 ppmv NO_2 (for 24 h) led to slightly more increase in iron fraction solubility, when compared to reaction with 2.5 ± 0.1 ppmv NO_2. For heterogeneous reaction with 2.5 ± 0.1 ppmv NO_2, there was no significant change in iron fractional solubility with reaction time or RH. This is consistent with our observation that particulate nitrate did not significantly vary with reaction time and RH, as discussed in Section 3.2.1.

Fig. 7c−d suggest that increase in iron fractional solubility was small and even insignificant for magnetite and goethite due to heterogeneous reaction with 2.5 ± 0.1 ppmv NO_2 up to 24 h.

Table 1
Average reactive uptake coefficients of NO_2 in the first 3 h for the three minerals.

RH	hematite [a]	hematite [b]	magnetite [b]	goethite [b]
	$(\times 10^{-9})$	$(\times 10^{-8})$	$(\times 10^{-8})$	$(\times 10^{-8})$
0%	5.13 ± 0.34	1.09 ± 0.15		
30%	4.73 ± 0.61	1.35 ± 0.22	2.91 ± 0.42	4.83 ± 0.94
60%	4.80 ± 0.44	1.20 ± 0.48	2.70 ± 0.60	4.03 ± 0.32
90%	4.93 ± 0.69	1.21 ± 0.38		

[a] $[NO_2] = 15 \pm 1$ ppmv
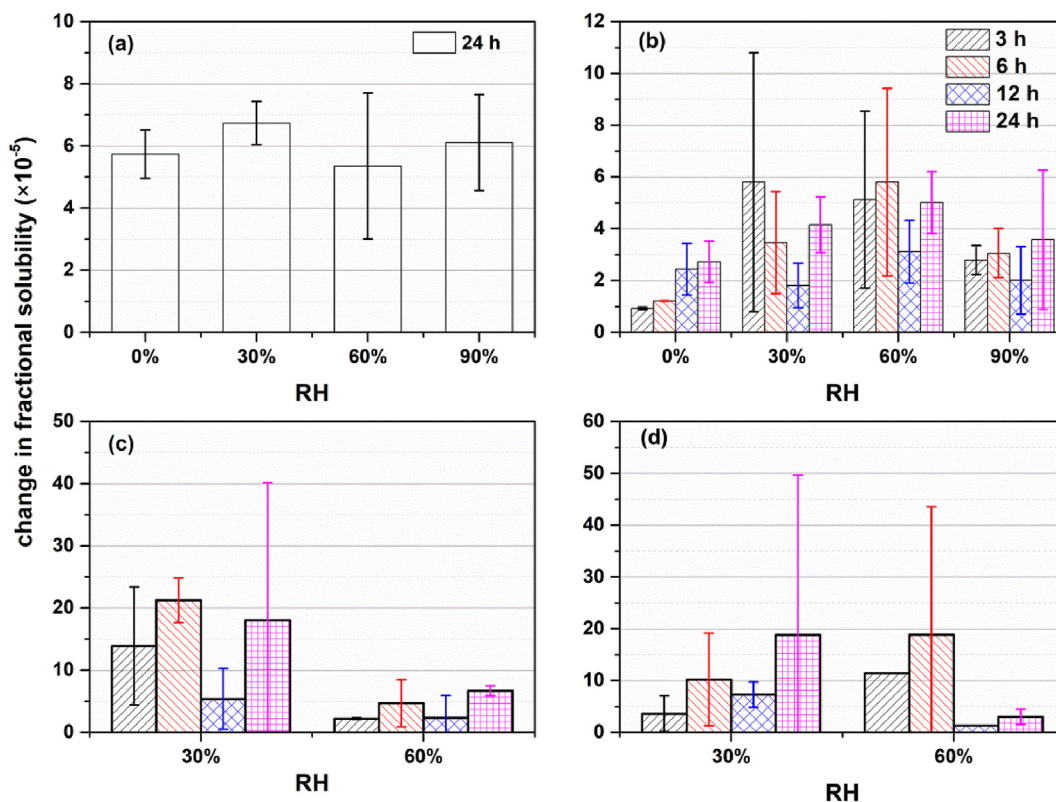[b] $[NO_2] = 2.5 \pm 0.1$ ppmv

Fig. 7. Changes in iron fractional solubility due to heterogeneous reaction with NO_2. (a) Heterogeneous reaction of hematite with 15 ± 1 ppmv NO_2 for 24 h; (b–d) heterogeneous reactions of (b) hematite, (c) magnetite and (d) goethite with 2.5 ± 0.1 ppmv NO_2 for 3, 6, 12 and 24 h.

Furthermore, the average mole ratios of changes in soluble iron to nitrate formed were significantly smaller than 0.1 for heterogeneous reaction of the three minerals with NO_2. In a previous study (Cartledge et al., 2015), hematite, magnetite and goethite were exposed to 5 ppmv SO_2 at 23% and 98% RH for 24 h. Similar to our work, Cartledge et al. (2015) found that heterogeneous reaction of SO_2 did not significantly increase iron fractional solubility of the three minerals. Large errors were observed for results presented in Fig. 7, mainly because iron solubility of fresh and aged mineral samples was very small.

4. Conclusion and implications

Heterogeneous reactions of mineral dust with nitrogen oxides would change the abundance of trace gases, modify aerosol composition and physiochemical properties, and affect solubilities of iron contained by mineral dust. However, the impacts of heterogeneous reaction of NO_2 with mineral dust on nitrate formation and iron solubility have not been well understood. In this work, heterogeneous reactions of NO_2 (15 ± 1 and 2.5 ± 0.1 ppmv, equal to $\sim 3.7 \times 10^{14}$ and $\sim 6.2 \times 10^{13}$ molecule cm^{-3}) with hematite, magnetite and goethite at different RH (0–90%) were investigated under atmospherically relevant conditions, and the amount of particulate nitrate formed and change in soluble iron were measured as a function of reaction time up to 24 h.

For hematite and magnetite, particle surface was completely deactivated in 12 h or less after exposure to 2.5 ± 0.1 ppmv NO_2, and increase in the amount of formed nitrate was only observed when RH was increased from 60% to 90%; for comparison, goethite surface was not fully saturated after exposure to 2.5 ± 0.1 ppmv NO_2 for 24 h, and increase in RH from 30% to 60% led to more nitrate being

formed. Nitrate yields were largest for goethite, and after reaction with 2.5 ± 0.1 ppmv NO_2 for 24 h, the mass ratio of formed nitrate to that of unreacted mineral was around 1% for goethite. In addition, the average reactive uptake coefficients of NO_2 in the first 3 h were found to be $< 5 \times 10^{-8}$ for all the three minerals, suggesting that their heterogeneous reactivities towards NO_2 are very low. Our results imply that the contribution of heterogeneous reaction of NO_2 with the three Fe-containing minerals (hematite, magnetite and goethite) to formation of aerosol nitrate would probably be minor, though the quantitative effects should be further assessed using numerical simulations.

The iron fractional solubility for unreacted hematite, magnetite and goethite were found to be approximately in the range of (1-10) $\times 10^{-5}$. After heterogeneous reaction with 2.5 ± 0.1 ppmv NO_2 for 24 h, the increase in iron fractional solubilities was very small and in some cases even insignificant. To our knowledge, our work is the first study which investigated the impact of heterogeneous reaction with NO_2 on iron solubility for mineral dust, and the impact was found to be small. It is unclear yet if heterogeneous reaction with NO_2 would significantly increase iron solubility of clay minerals and authentic desert particles. Furthermore, heterogeneous reaction of NO_2 with mineral dust can be photo-enhanced (Ndour et al., 2008, 2009), and therefore heterogeneous reaction of NO_2 under irradiation may lead to more significant increase in iron solubility for mineral dust. Compared to NO_2, HNO_3 (Hanisch and Crowley, 2001; Vlasenko et al., 2009) and N_2O_5 (Tang et al., 2012, 2014) are more reactive toward mineral dust; as a result, the effects of heterogeneous reactions with HNO_3 and N_2O_5 on iron solubility may be significant for mineral dust and hence deserve investigation.

Acknowledgment

Appendix A. Supplementary data

Supplementary data to this article can be found online at https://doi.org/10.1016/j.chemosphere.2019.125273.

References

Avila, A., Queralt-Mitjans, I., Alarcón, M., 1997. Mineralogical composition of African dust delivered by red rains over northeastern Spain. J. Geophys. Res.-Atmos. 102, 21977—21996.

Baker, A.R., French, M., Linge, K.L., 2006. Trends in aerosol nutrient solubility along a west—east transect of the Saharan dust plume. Geophys. Res. Lett. 33, L07805. https://doi.org/10.1029/2005GL024764.

Baker, A.R., Croot, P.L., 2010. Atmospheric and marine controls on aerosol iron solubility in seawater. Mar. Chem. 120, 4—13.

Baltrusaitis, J., Jayaweera, P.M., Grassian, V.H., 2009. XPS study of nitrogen dioxide adsorption on metal oxide particle surfaces under different environmental conditions. Phys. Chem. Chem. Phys. 11, 8295—8305.

Baltrusaitis, J., Chen, H., Rubasinghege, G., Grassian, V.H., 2012. Heterogeneous atmospheric chemistry of lead oxide particles with nitrogen dioxide increases lead solubility: environmental and health implications. Environ. Sci. Technol. 46, 12806—12813.

Bedjanian, Y., Romanias, M.N., El Zein, A., 2013. Interaction of OH radicals with Arizona test dust: uptake and products. J. Phys. Chem. A 117, 393—400.

Boyd, P.W., Jickells, T., Law, C.S., Blain, S., Boyle, E.A., Buesseler, K.O., Coale, K.H., Cullen, J.J., de Baar, H.J.W., Follows, M., Harvey, M., Lancelot, C., Levasseur, M., Owens, N.P.J., Pollard, R., Rivkin, R.B., Sarmiento, J., Schoemann, V., Smetacek, V., Takeda, S., Tsuda, A., Turner, S., Watson, A.J., 2007. Mesoscale iron enrichment experiments 1993-2005: synthesis and future directions. Science 315, 612—617.

Boyd, P.W., Ellwood, M.J., 2010. The biogeochemical cycle of iron in the ocean. Nat. Geosci. 3, 675—682.

Cartledge, B.T., Marcotte, A.R., Herckes, P., Anbar, A.D., Majestic, B.J., 2015. The impact of particle size, relative humidity, and sulfur dioxide on iron solubility in simulated atmospheric marine aerosols. Environ. Sci. Technol. 49, 7179—7187.

Chen, H., Grassian, V.H., 2013. Iron dissolution of dust source materials during simulated acidic processing: the effect of sulfuric, acetic, and oxalic acids. Environ. Sci. Technol. 47 https://doi.org/10.1021/acs.est.5b02452.

Crowley, J.N., Ammann, M., Cox, R.A., Hynes, R.G., Jenkin, M.E., Mellouki, A., Rossi, M.J., Troe, J., Wallington, T.J., 2010. Evaluated kinetic and photochemical data for atmospheric chemistry: volume V — heterogeneous reactions on solid substrates. Atmos. Chem. Phys. 10, 9059—9223.

Cziczo, D.J., Froyd, K.D., Hoose, C., Jensen, E.J., Diao, M., Zondlo, M.A., Smith, J.B., Twohy, C.H., Murphy, D.M., 2013. Clarifying the dominant sources and mechanisms of cirrus cloud formation. Science 340, 1320—1324.

Dentener, F.J., Carmichael, G.R., Zhang, Y., Lelieveld, J., Crutzen, P.J., 1996. Role of mineral aerosol as a reactive surface in the global troposphere. J. Geophys. Res.-Atmos. 101, 22869—22889.

Fu, H., Lin, J., Shang, G., Dong, W., Grassian, V.H., Carmichael, G.R., Li, Y., Chen, J., 2012. Solubility of iron from combustion source particles in acidic media linked to iron speciation. Environ. Sci. Technol. 46, 11119—11127.

Goodman, A.L., Bernard, E.T., Grassian, V.H., 2001. Spectroscopic study of nitric acid and water adsorption on oxide particles: enhanced nitric acid uptake kinetics in the presence of adsorbed water. J. Phys. Chem. A 105, 6443—6457.

Ginoux, P., Prospero, J.M., Gill, T.E., Hsu, N.C., Zhao, M., 2012. Global-scale attribution of anthropogenic and natural dust sources and their emission rates based on MODIS Deep Blue aerosol products. Rev. Geophys. 50, RG3005. https://doi.org/10.1029/2012RG000388.

Hanisch, F., Crowley, J.N., 2001. Heterogeneous reactivity of gaseous nitric acid on Al$_2$O$_3$, CaCO$_3$, and atmospheric dust samples: a knudsen cell study. J. Phys. Chem. A 105, 3096—3106.

Hettiarachchi, E., Hurab, O., Rubasinghege, G., 2018a. Atmospheric processing and iron mobilization of ilmenite: iron-containing ternary oxide in mineral dust aerosol. J. Phys. Chem. A 122, 1291—1302.

Hettiarachchi, E., Reynolds, R.L., Goldstein, H.L., Moskowitz, B., Rubasinghege, G., 2018b. Iron dissolution and speciation in atmospheric mineral dust: metal-metal synergistic and antagonistic effects. Atmos. Environ. 187, 417—423.

Hettiarachchi, E., Reynolds, R.L., Goldstein, H.L., Moskowitz, B., Rubasinghege, G., 2019. Bioavailable iron production in airborne mineral dust: control by chemical composition and solar flux. Atmos. Environ. 205, 90—102.

Huneeus, N., Schulz, M., Balkanski, Y., Griesfeller, J., Prospero, J., Kinne, S., Bauer, S., Boucher, O., Chin, M., Dentener, F., Diehl, T., Easter, R., Fillmore, D., Ghan, S., Ginoux, P., Grini, A., Horowitz, L., Koch, D., Krol, M.C., Landing, W., Liu, X., Mahowald, N., Miller, R., Morcrette, J.J., Myhre, G., Penner, J., Perlwitz, J., Stier, P., Takemura, T., Zender, C.S., 2011. Global dust model intercomparison in AeroCom phase I. Atmos. Chem. Phys. 11, 7781—7816.

Ito, A., Myriokefalitakis, S., Kanakidou, M., Mahowald, N.M., Scanza, R.A., Hamilton, D.S., Baker, A.R., Jickells, T., Sarin, M., Bikkina, S., Gao, Y., Shelley, R.U., Buck, C.S., Landing, W.M., Bowie, A.R., Perron, M.M.G., Guieu, C., Meskhidze, N., Johnson, M.S., Feng, Y., Kok, J.F., Nenes, A., Duce, R.A., 2019. Pyrogenic iron: the missing link to high iron solubility in aerosols. Sci. Adv. 5, eaau7671 https://doi.org/10.1126/sciadv.aau7671.

Jickells, T.D., An, Z.S., Andersen, K.K., Baker, A.R., Bergametti, G., Brooks, N., Cao, J.J., Boyd, P.W., Duce, R.A., Hunter, K.A., Kawahata, H., Kubilay, N., laRoche, J., Liss, P.S., Mahowald, N., Prospero, J.M., Ridgwell, A.J., Tegen, I., Torres, R., 2005. Global iron connections between desert dust. Ocean Biogeochemistry, and Climate, Science 308, 67—71.

Journet, E., Desboeufs, K.V., Caquineau, S., Colin, J.-L., 2008. Mineralogy as a critical factor of dust iron solubility. Geophys. Res. Lett. 35, L07805. https://doi.org/10.1029/2007gl031589.

Kebede, M.A., Bish, D.L., Losovyj, Y., Engelhard, M.H., Raff, J.D., 2016. The role of iron-bearing minerals in NO$_2$ to HONO conversion on soil surfaces. Environ. Sci. Technol. 50, 8649—8660.

Kok, J.F., Ward, D.S., Mahowald, N.M., Evan, A.T., 2018. Global and regional importance of the direct dust-climate feedback. Nat. Commun. 9, 241. https://doi.org/10.1038/s41467-017-02620-y.

Krueger, B.J., Grassian, V.H., Laskin, A., Cowin, J.P., 2003. The transformation of solid atmospheric particles into liquid droplets through heterogeneous chemistry: Laboratory insights into the processing of calcium containing mineral dust aerosol in the troposphere. Geophys. Res. Lett. 30 (3), 1148. https://doi.org/10.1029/2002GL016563.

Kulkarni, G., Zhang, K., Zhao, C., Nandasiri, M., Shutthanandan, V., Liu, X., Fast, J., Berg, L., 2015. Ice formation on nitric acid-coated dust particles: Laboratory and modeling studies. J. Geophys. Res.-Atmos. 120, 7682—7698.

Lafon, S., Rajot, J.-L., Alfaro, S.C., Gaudichet, A., 2004. Quantification of iron oxides in desert aerosol. Atmos. Environ. 38, 1211—1218.

Laskin, A., Wietsma, T.W., Krueger, B.J., Grassian, V.H., 2005. Heterogeneous chemistry of individual mineral dust particles with nitric acid: a combined CCSEM/EDX, ESEM, and ICP-MS study. J. Geophys. Res.-Atmos. 110, D10208. https://doi.org/10.1029/2004JD005206.

Li, H., Zhu, T., Ding, J., Chen, Q., Xu, B., 2006. Heterogeneous reaction of NO$_2$ on the surface of NaCl particles. Sci. China, Ser. B: Chemistry 49, 371—378.

Li, H.J., Zhu, T., Zhao, D.F., Zhang, Z.F., Chen, Z.M., 2010. Kinetics and mechanisms of heterogeneous reaction of NO$_2$ on CaCO$_3$ surfaces under dry and wet conditions. Atmos. Chem. Phys. 10, 463—474.

Liu, Y., Han, C., Ma, J., Bao, X., He, H., 2015. Influence of relative humidity on heterogeneous kinetics of NO$_2$ on kaolin and hematite. Phys. Chem. Chem. Phys. 17, 19424—19431.

Liu, C., Ma, Q.X., He, H., He, G.Z., Ma, J.Z., Liu, Y.C., Wu, Y., 2017. Structure-activity relationship of surface hydroxyl groups during NO$_2$ adsorption and transformation on TiO$_2$ nanoparticles. Environ. Sci.: Nano 4, 2388—2394.

Luo, C., Mahowald, N., Bond, T., Chuang, P.Y., Artaxo, P., Siefert, R., Chen, Y., Schauer, J., 2008. Combustion iron distribution and deposition. Glob. Biogeochem. Cycles 22, GB1012. https://doi.org/10.1029/2007gb002964.

Ma, Q.X., He, H., Liu, Y.C., 2010. In situ DRIFTS study of hygroscopic behavior of mineral aerosol. J. Environ. Sci. 22, 555—560.

Ma, Q., Liu, Y., Liu, C., He, H., 2012. Heterogeneous reaction of acetic acid on MgO, α-Al$_2$O$_3$, and CaCO$_3$ and the effect on the hygroscopic behaviour of these particles. Phys. Chem. Chem. Phys. 14, 8403—8409.

Mahowald, N.M., Baker, A.R., Bergametti, G., Brooks, N., Duce, R.A., Jickells, T.D., Kubilay, N., Prospero, J.M., Tegen, I., 2005. Atmospheric global dust cycle and iron inputs to the ocean. Glob. Biogeochem. Cycles 19, GB4025. https://doi.org/10.1029/2004GB002402.

Mahowald, N., 2011. Aerosol indirect effect on biogeochemical cycles and climate. Science 334, 794—796.

Mahowald, N.M., Hamilton, D.S., Mackey, K.R.M., Moore, J.K., Baker, A.R., Scanza, R.A., Zhang, Y., 2018. Aerosol trace metal leaching and impacts on marine microorganisms. Nat. Commun. 9, 2614. https://doi.org/10.1038/s41467-018-04970-7.

Morton, P.L., Landing, W.M., Hsu, S.-C., Milne, A., Aguilar-Islas, A.M., Baker, A.R., Bowie, A.R., Buck, C.S., Gao, Y., Gichuki, S., Hastings, M.G., Hatta, M., Johansen, A.M., Losno, R., Mead, C., Patey, M.D., Swarr, G., Vandermark, A., Zamora, L.M., 2013. Methods for the sampling and analysis of marine aerosols: results from the 2008 GEOTRACES aerosol intercalibration experiment. Limnol Oceanogr. Methods 11, 62—78.

Ndour, M., D'Anna, B., George, C., Ka, O., Balkanski, Y., Kleffmann, J., Stemmler, K., Ammann, M., 2008. Photoenhanced uptake of NO$_2$ on mineral dust: Laboratory experiments and model simulations. Geophys. Res. Lett. 35, L05812. https://doi.org/10.1029/2007GL032006.

Ndour, M., Nicolas, M., D'Anna, B., Ka, O., George, C., 2009. Photoreactivity of NO$_2$ on mineral dusts originating from different locations of the Sahara desert. Phys. Chem. Chem. Phys. 11, 1312—1319.

Ooki, A., Nishioka, J., Ono, T., Noriki, S., 2009. Size dependence of iron solubility of Asian mineral dust particles. J. Geophys. Res.-Atmos. 114, D03202. https://

doi.org/10.1029/2008JD010804.

Schroth, A.W., Crusius, J., Sholkovitz, E.R., Bostick, B.C., 2009. Iron solubility driven by speciation in dust sources to the ocean. Nat. Geosci. 2, 337–340.

Schulz, M., Prospero, J.M., Baker, A.R., Dentener, F., Ickes, L., Liss, P.S., Mahowald, N.M., Nickovic, S., García-Pando, C.P., Rodríguez, S., Sarin, M., Tegen, I., Duce, R.A., 2012. Atmospheric transport and deposition of mineral dust to the ocean: implications for research needs. Environ. Sci. Technol. 46, 10390–10404.

Shi, J.-H., Zhang, J., Gao, H.-W., Tan, S.-C., Yao, X.-H., Ren, J.-L., 2013. Concentration, solubility and deposition flux of atmospheric particulate nutrients over the Yellow Sea. Deep-Sea Res. Part II Top. Stud. Oceanogr. 97, 43–50.

Shi, Z., Shao, L., Jones, T.P., Lu, S., 2005. Microscopy and mineralogy of airborne particles collected during severe dust storm episodes in Beijing, China. J. Geophys. Res.-Atmos. 110, D01303. https://doi.org/10.1029/2004JD005073.

Shi, Z., Krom, M.D., Bonneville, S., Baker, A.R., Jickells, T.D., Benning, L.G., 2009. formation of iron nanoparticles and increase in iron reactivity in mineral dust during simulated cloud processing. Environ. Sci. Technol. 43, 6592–6596.

Shi, Z., Krom, M.D., Bonneville, S., Baker, A.R., Bristow, C., Drake, N., Mann, G., Carslaw, K., McQuaid, J.B., Jickells, T., Benning, L.G., 2011a. Influence of chemical weathering and aging of iron oxides on the potential iron solubility of Saharan dust during simulated atmospheric processing. Glob. Biogeochem. Cycles 25, GB2010. https://doi.org/10.1029/2010GB003837.

Shi, Z., Woodhouse, M.T., Carslaw, K.S., Krom, M.D., Mann, G.W., Baker, A.R., Savov, I., Fones, G.R., Brooks, B., Drake, N., Jickells, T.D., Benning, L.G., 2011b. Minor effect of physical size sorting on iron solubility of transported mineral dust. Atmos. Chem. Phys. 11, 8459–8469.

Shi, Z., Krom, M.D., Jickells, T.D., Bonneville, S., Carslaw, K.S., Mihalopoulos, N., Baker, A.R., Benning, L.G., 2012. Impacts on iron solubility in the mineral dust by processes in the source region and the atmosphere: a review. Aeolian Res 5, 21–42.

Sholkovitz, E.R., Sedwick, P.N., Church, T.M., Baker, A.R., Powell, C.F., 2012. Fractional solubility of aerosol iron: synthesis of a global-scale data set. Geochem. Cosmochim. Acta 89, 173–189.

Solmon, F., Chuang, P.Y., Meskhidze, N., Chen, Y., 2009. Acidic processing of mineral dust iron by anthropogenic compounds over the north Pacific Ocean. J. Geophys. Res.-Atmos. 114, D02305. https://doi.org/10.1029/2008JD010417.

Sullivan, R.C., Guazzotti, S.A., Sodeman, D.A., Prather, K.A., 2007. Direct observations of the atmospheric processing of Asian mineral dust. Atmos. Chem. Phys. 7, 1213–1236.

Tagliabue, A., Bowie, A.R., Boyd, P.W., Buck, K.N., Johnson, K.S., Saito, M.A., 2017. The integral role of iron in ocean biogeochemistry. Nature 543, 51–59.

Tan, F., Tong, S., Jing, B., Hou, S., Liu, Q., Li, K., Zhang, Y., Ge, M., 2016. Heterogeneous reactions of NO_2 with $CaCO_3$–$(NH_4)_2SO_4$ mixtures at different relative humidities. Atmos. Chem. Phys. 16, 8081–8093.

Tang, M.J., Thieser, J., Schuster, G., Crowley, J.N., 2012. Kinetics and mechanism of the heterogeneous reaction of N_2O_5 with mineral dust particles. Phys. Chem. Chem. Phys. 14, 8551–8561.

Tang, M.J., Schuster, G., Crowley, J.N., 2014. Heterogeneous reaction of N_2O_5 with illite and Arizona test dust particles. Atmos. Chem. Phys. 14, 245–254.

Tang, M., Cziczo, D.J., Grassian, V.H., 2016. Interactions of water with mineral dust aerosol: water adsorption, hygroscopicity, cloud condensation, and ice nucleation. Chem. Rev. 116, 4205–4259.

Tang, M., Huang, X., Lu, K., Ge, M., Li, Y., Cheng, P., Zhu, T., Ding, A., Zhang, Y., Gligorovski, S., Song, W., Ding, X., Bi, X., Wang, X., 2017. Heterogeneous reactions of mineral dust aerosol: implications for tropospheric oxidation capacity. Atmos. Chem. Phys. 17, 11727–11777.

Underwood, G.M., Miller, T.M., Grassian, V.H., 1999. Transmission FT-IR and Knudsen cell study of the heterogeneous reactivity of gaseous nitrogen dioxide on mineral oxide particles. J. Phys. Chem. A 103, 6184–6190.

Underwood, G.M., Li, P., Usher, C.R., Grassian, V.H., 2000. Determining accurate kinetic parameters of potentially important heterogeneous atmospheric reactions on solid particle surfaces with a knudsen cell reactor. J. Phys. Chem. A 104, 819–829.

Usher, C.R., Michel, A.E., Grassian, V.H., 2003. Reactions on mineral dust. Chem. Rev. 103, 4883–4940.

Vlasenko, A., Huthwelker, T., Gaggeler, H.W., Ammann, M., 2009. Kinetics of the heterogeneous reaction of nitric acid with mineral dust particles: an aerosol flow tube study. Phys. Chem. Chem. Phys. 11, 7921–7930.

Wang, Z., Fu, H., Zhang, L., Song, W., Chen, J., 2017. Ligand-promoted photoreductive dissolution of goethite by atmospheric low-molecular dicarboxylates. J. Phys. Chem. A 121, 1647–1656.

Wang, Z., Li, R., Cui, L., Fu, H., Lin, J., Chen, J., 2018. Characterization and acid-mobilization study for typical iron-bearing clay mineral. J. Environ. Sci. 71, 222–232.

Wijenayaka, L.A., Rubasinghege, G., Baltrusaitis, J., Grassian, V.H., 2012. Surface Chemistry of α-FeOOH Nanorods and Microrods with Gas- Phase Nitric Acid and Water Vapor: Insights into the Role of Particle Size, Surface Structure, and Surface Hydroxyl Groups in the Adsorption and Reactivity of α-FeOOH with Atmospheric Gases. J. Phys. Chem. C 116, 12566–12577.